

Experimental observation of cnoidal waveform of nonlinear dust acoustic waves

Bin Liu, J. Goree, and T. M. Flanagan

Department of Physics and Astronomy, The University of Iowa, Iowa City, Iowa 52242, USA

Abhijit Sen

Institute for Plasma Research, Bhat, Gandhinagar 382 428, India

Sanat Kumar Tiwari

Department of Physics, Indian Institute of Technology Jammu, Jammu - 181 121, J&K, India

Gurudas Ganguli and Chris Crabtree

Naval Research Laboratory, Washington, DC 20375, USA

(Dated: October 1, 2018)

The experimentally measured waveform of nonlinear dust acoustic waves in a plasma is shown to be accurately described by a cnoidal function. This function, which is predicted by nonlinear theory, has broad minima and narrow peaks. Fitting the experimental waveforms to the cnoidal function also provides a measure of the wave's nonlinearity, namely, the elliptical parameter k . By characterizing experimental results at various wave amplitudes, we confirm that the parameter k increases and approaches a maximum value of unity, as the wave amplitude is increased. The underlying theory that predicts the cnoidal waveform as an exact solution of a Korteweg-de Vries model equation takes account of the streaming ions that are responsible for the spontaneous excitation of the dust acoustic waves.

I. INTRODUCTION

Waves can easily grow to be nonlinear in dusty plasmas [1–14]. A dusty plasma contains microparticles, i.e., dust grains, which absorb electrons and ions, and thereby gain a large negative charge. When a cloud of these microparticles undergoes a compression or rarefaction, electric fields arise, and this can lead to the propagation of a density wave, which is called the dust acoustic wave (DAW) [15–32]. At low amplitudes, the DAW obeys a linear dispersion relation that has been widely studied; this dispersion relation can depend on physical processes including not only dust particle charge and gas friction, but also other effects such as ion-neutral friction and ion kinetic effects [30]. The amplitude of the DAW can easily attain large amplitudes, due to the large electric forces experienced by the microparticles. Wave electric fields can result in these large forces due to the large charges on each microparticle, so that the microparticle motion associated with the waves can easily become nonlinear. In such nonlinear waves, the dust number density can fluctuate with a large percentage, as can be seen easily in an experiment by video imaging [24, 25]. A common mechanism of exciting the waves in an experiment is energy input from flowing ions [26]. The DAWs have been observed in numerous experiments, for example [16–25, 33–37] including those under microgravity conditions provided by parabolic flights [34–37].

Here we use experimental data to demonstrate that the waveform of these nonlinear dust acoustic waves has the shape of a cnoidal function. This cnoidal function, which will be defined in Sec. II, has been predicted theoretically for nonlinear waves in various physical systems [38–43]. Theories have also been developed specifically for dusty

plasmas [44–50], under various assumptions, predicting cnoidal solutions for nonlinear waves. For example, Yadav *et al.* [44, 45] derived a theory predicting a cnoidal solution for dust acoustic waves under an assumption that included Boltzmann electrons and ions and cold dust with fluctuating charges. Saini *et al.* [49] used a model consisting of two components of superthermal electrons to study cnoidal solutions for nonlinear dust ion-acoustic waves while Tolba *et al.* [50] studied cnoidal forms of dust acoustic waves in positively charged dusty plasmas.

The connection between the cnoidal wave function and the physical system is that the oscillations in the dusty plasma can sometimes be modeled by the classical Korteweg de Vries (KdV) equation, and it is this equation that allows a cnoidal solution. One can derive the KdV equation from a fluid description of the plasma, and the derivation can result in essentially the same KdV equation even if one makes varying assumptions; different assumptions made deriving the equation show up as modifications in the coefficients of the equation. In Sec. VI we will show that the KdV equation can be obtained for nonlinear DAWs not only with the original assumptions of Yadav *et al.* [44, 45], but also if the assumptions are altered to make the ion flow less responsive to changes in the local electric potential. This derivation leads us to remark that the KdV description of nonlinear waves is robust; in particular, it is robust in the sense that it is not greatly sensitive to all the physical assumptions.

The experimental literature for cnoidal waveform is more sparse than for the theory. We are aware of only one previous plasma experiment that tested the cnoidal solution; that experiment was for nonlinear drift waves [40] in a non-dusty plasma. Other physical systems that have been studied experimentally, for the cnoidal shape of

their nonlinear waves, include surface gravity waves in shallow water [38, 39, 43], and laser interference fringes in the photorefractive bismuth titanate oxide (BTO) crystal [42].

In this paper, we find that the cnoidal wave solution accurately describes the waveform of nonlinear dust acoustic waves in a ground-based experiment. We will analyze the data from a previous experiment [25], where the level of the wave's nonlinearity was regulated by adjusting the damping level due to gas drag. In the present analysis, we will fit the experimental data to a cnoidal wave solution of an appropriate KdV equation, derived in Sec. VI. This fit will also yield a useful parameter k to quantify the nonlinearity of the waves. As a measure of nonlinearity, we will also compare the cnoidal parameter k to the total harmonic distortion, which was reported in the previous experiment in Ref. [24].

II. THEORETICAL FORMULA

The cnoidal wave solution of the KdV equation can be represented in the form,

$$\phi(x, t) = \beta_2 + (\beta_3 - \beta_2)cn^2 \left[2K(k) \left(\frac{x}{\lambda} + ft \right); k \right], \quad (1)$$

where, β_2 and β_3 are wave's minimum and maximum amplitudes, respectively; the function cn is one of the Jacobi elliptic functions, with an elliptic parameter $k = \sqrt{(\beta_3 - \beta_2)/(\beta_3 - \beta_1)}$, where β_1 is a constant; $K(k)$ is the complete elliptic integral of the first kind; λ and f are the wavelength and wave frequency, respectively.

In this paper, we will test Eq. (1) with experimental waveform data. This test will also generate a value for the elliptic parameter k in Eq. (1). The parameter k characterizes the shape of the cnoidal function. For $k = 0$ the cnoidal solution becomes a cosine function, while for values close to unity the cnoidal function gets sharpened peaks and flattened bottoms.

III. EXPERIMENT

Here we review a few key points about the experiment. Further details are found in Ref. [24]. In the experiment, a three-dimensional dust cloud was trapped using a glass box in an Argon plasma. The plasma was sustained by a radio-frequency (13.6 MHz) voltage applied between a horizontal lower electrode and a grounded vacuum chamber. Ten runs were performed, at gas pressures ranging from 372 to 420 mtorr. Gas flow was negligible, especially in our region of interest within the glass box. Polymer microspheres of 4.8 μm diameter were introduced into the plasma, and they were electrically confined by natural electric fields, which were enhanced in the horizontal

direction by the glass box, which was open on the top. The fields' vertical component provided levitation of the particles and it also drove a downward ion flow that could excite DAWs. Aside from these waves, there was no general motion of the dust particles in the vertical direction.

The dust cloud was imaged with a digital video camera viewing from the side. Here, we will analyze the image data from the experiment, which were recorded at a speed of 500 frames/s. In Fig. 1, we show snapshots of the dust cloud, which exhibits compressive wave fronts, which are horizontal and propagate. As discussed in Ref. [24], the image intensity is linearly related to the number density of dust particles, due to the design of the experiment.

The degree of the wave's nonlinearity in the experiment was regulated by adjusting the gas pressure. The gas pressure was different in each of the ten experimental runs. The wave was self-excited by ion flow, and this energy input to the wave competed with gas frictional damping. As seen in the snapshots of Fig. 1(f), for the gas pressure of $p = 420$ mTorr, no wave was detectable. By reducing the pressure slightly to 416 mTorr, Fig. 1(e), waves were excited; the wave amplitude was significant and even attained a nonlinear amplitude. Further small reductions in the gas pressure yielded even higher wave amplitudes, Fig. 1(a)-1(d). The gas pressure can be used to calculate a damping rate, in s^{-1} , using the formula [6],

$$\nu_E = 2333 \frac{\delta_E}{\rho r_d} p \sqrt{\frac{Z_{gas}}{T_{gas}}}, \quad (2)$$

where the Epstein constant δ_E is in the range 1.0 to 1.442. In Eq. (2), ρ is dust particle's mass density in kg/m^3 , r_d is particle radius in microns, p is gas pressure in mTorr, T_{gas} is gas temperature in K, and Z_{gas} is the atomic mass of gas molecule. Here, we use $\delta_E = 1.26$, as in Ref. [6], $\rho = 1510$ kg/m^3 for the particle's mass density, $Z_{gas} = 39.948$ for Argon, and $T_{gas} = 290$ K because the experiment was performed with a vacuum chamber at room temperature. Our calculated values for ν_E are presented in Table I. The damping rate was in a range from 112 to 125 s^{-1} . This level of damping rate significantly hinders the wave growth in the experimental system. An instability with a growth rate slightly greater than this damping rate, however, can overcome the friction and result in a substantial wave, as described in [24].

IV. ANALYSIS METHOD

A. Obtaining experimental waveform

Our analysis mainly centers on the waveforms of dust number density fluctuations, which we obtain from a sequence of video images. We exploit the linear relationship of image brightness and dust number density to calculate the density, in arbitrary units.

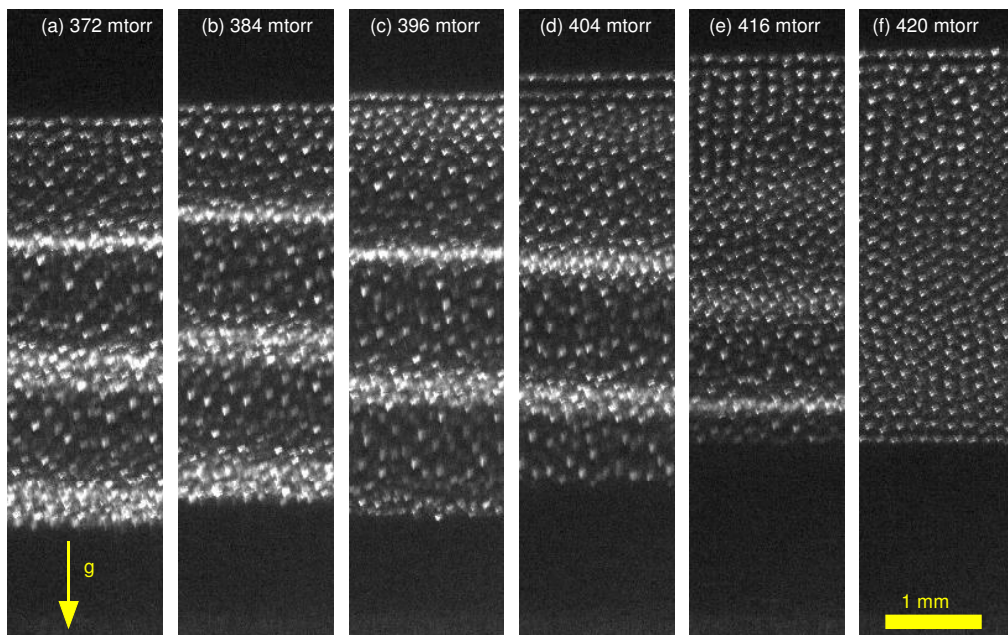


FIG. 1. Images of a cross section of a 3D dust cloud. Waves are seen in (a) to (e), as indicated by density compression and rarefaction (i.e., the spatial variation in pixel brightness). The observed wave propagated from the top downward, and the wave grew in amplitude as it propagated downward through the cloud. The series of images shown here, (a)-(f), are for six experiment runs, each for a different value of the damping rate, as controlled by gas pressure. Each panel is from one frame of a video.

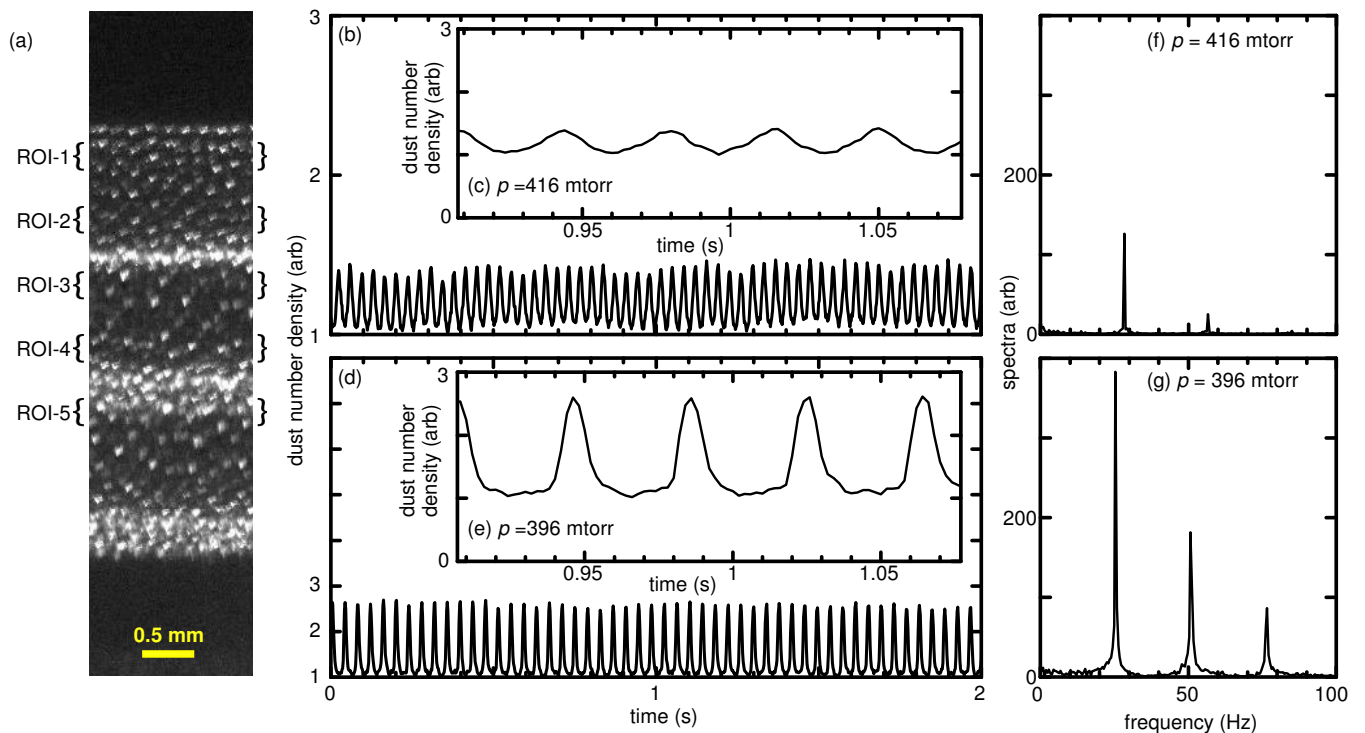


FIG. 2. (a) Regions of interest ROI-1 to ROI-5. These equally-spaced rectangles (1.65 by 0.26 mm) each span the image's width. The same five locations are used for the ROIs in all experimental runs. Within a ROI, for one video frame, we spatially average the pixel intensities, yielding a measure of local number density at a particular time, in arbitrary units. Repeating for a sequence of video frames yields a times series of local number density for an experimental run, as in (b) and (d), which are for ROI-3. The inset (c) is a zoomed view of a portion of (b). Fourier transforming the time series in (b) and (d) yields the spectra in (e) and (f), respectively.

For an image from one video frame, we choose a region of interest (ROI), as identified in Fig. 2(a). Within the rectangular boundary of the ROI, 1.65×0.26 mm, we spatially average the image intensity, yielding one instantaneous measure of the number density. We repeat this measurement for every frame of the recorded video data. In this way we obtain a raw waveform, with about 50 oscillations, as in Figs. 2(b) and 2(d).

In this experiment, the raw waveform had a frequency of about 26 Hz (i.e., a period of about 38.5 ms), and the peak-to-peak amplitude was typically 55% of the maximum value. The frequency (inverse period) was the result of the instability, which is responsible for the waves, having a growth rate that is greatest for a preferred wavelength, which can vary depending on the plasma conditions. For the same run, the frequency and amplitude were not constant; the period varied from 34.5 to 41.7 ms, and the peak-to-peak amplitude varied from 50% to 60% of the maximum value. These variations can arise because the wave was self-excited; the experimental setup did not include any measures to control the wave, such as external modulation to provide synchronization [28].

Due to these variations in the amplitude and period in the raw waveform, we processed the raw waveforms by averaging them to yield a smoothed waveform. This averaging process involved choosing ten non-overlapping segments, each starting at the same phase, which was a peak value. The segment lengths were such that they included approximately four wave periods. Averaging these ten segments yielded a smoothed waveform, like the examples shown in Fig. 3. The waveform is nearly sinusoidal only when the wave's amplitude is small, Fig. 3(e). At larger amplitude the waveform has distinctive sharpened peaks with a flattened bottom, Fig. 3(a)-3(d), indicating strong nonlinearity.

B. Determining wave's amplitude and frequency

We obtain the wave's amplitude and frequency by an inspection of the peaks in the smoothed waveform. The average of the peak values yields the maximum amplitude β_3 as defined in Eq. (1), while the average of the time interval between the peaks yields the frequency f . The minimum amplitude β_2 is obtained by finding the minimum of the waveform. We then calculate the peak-to-peak amplitude, $H = (\beta_3 - \beta_2)/\beta_2$, which is normalized by the minimum amplitude β_2 .

V. EXPERIMENTAL RESULTS

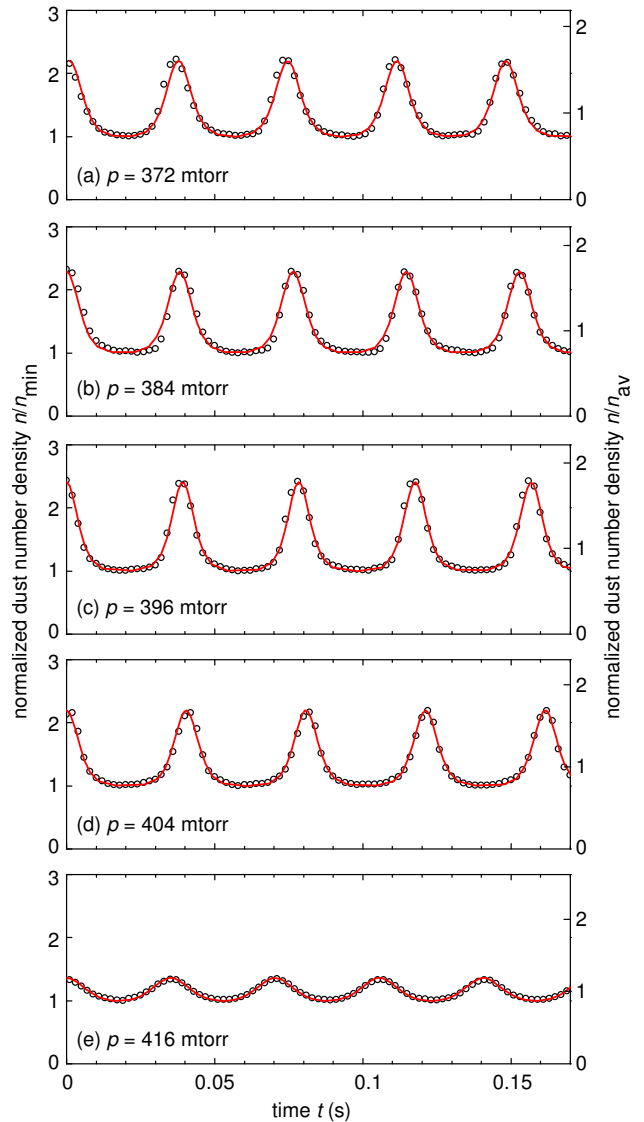


FIG. 3. Experimental waveform of dust number density n and cnoidal fit. (The normalized quantity plotted here is the dust number density, not the peak-to-peak amplitude Δn as in Table I.) The experimental data (circles) shown here are smoothed waveforms, obtained by an averaging of the raw waveform time series such as those in Figs. 2(b)-2(e). The dust number density data is normalized by the minimum n_{\min} (left axis) and the mean n_{av} (right axis) of the waveform. Different panels (a)-(e) correspond to different damping levels, as characterized by the damping rate ν_E , but for the same ROI-3. The fit is shown as continuous curves, computed using Eq. (3). The excellent agreement between the fitted and experimental data demonstrates that the cnoidal wave solution can accurately describe the waveforms of nonlinear dust acoustic waves. The values of k , f , and ν_E are presented in Table I.

A. Fitting

Our main result is a fit of the cnoidal function to the smoothed experimental waveforms, in Fig. 3. The data

TABLE I. Experimental parameters and results, for various gas pressure p and regions of interest (ROIs). The position of each ROI is marked in Fig. 2(a). The peak-to-peak amplitude Δn is presented two ways, $\Delta n/n_{av}$ and $H = \Delta n/n_{min}$, normalized by the mean n_{av} and the minimum n_{min} , respectively. The damping rate ν_E , normalized by the frequency f , is calculated using Eq. (2) for each gas pressure. As measures of the wave's nonlinearity, both the total harmonic distortion THD and the cnoidal fit parameter k are presented.

Gas pressure p (mtorr)	ROI	Analysis of waveform			Gas damping	Nonlinearity	cnoidal fit
		$\Delta n/n_{av}$	H	f (Hz)	$\nu_E/2\pi f$	THD (%)	k
372	ROI-3	0.88	1.20	27.1	0.66	48.0	0.989
380	ROI-3	0.98	1.34	26.6	0.68	72.7	0.995
384	ROI-3	0.95	1.29	26.1	0.70	55.9	0.993
392	ROI-3	1.02	1.40	25.9	0.73	48.6	0.995
396	ROI-3	1.04	1.41	25.4	0.75	52.5	0.997
400	ROI-3	0.90	1.16	25.3	0.76	81.7	0.997
404	ROI-1	0.27	0.30	24.6	0.79	32.2	0.890
	ROI-2	0.45	0.53	25.0	0.77	39.5	0.949
	ROI-3	0.92	1.20	24.7	0.78	57.7	0.996
	ROI-4	0.83	1.12	24.9	0.78	69.0	0.986
	ROI-5	0.78	1.07	24.8	0.78	50.6	0.959
408	ROI-1	0.23	0.26	24.6	0.79	19.0	0.812
	ROI-2	0.29	0.33	24.4	0.80	25.5	0.857
	ROI-3	0.59	0.72	24.4	0.80	37.8	0.985
	ROI-4	0.79	1.02	24.6	0.79	53.2	0.993
	ROI-5	0.99	1.39	24.4	0.80	48.4	0.995
412	ROI-1	0.14	0.15	28.2	0.70	10.0	0.708
	ROI-2	0.24	0.27	28.7	0.69	32.1	0.863
	ROI-3	0.44	0.53	28.5	0.69	55.2	0.966
	ROI-4	0.66	0.84	28.6	0.69	74.2	0.988
	ROI-5	0.58	0.75	28.4	0.69	67.5	0.938
416	ROI-1	0.13	0.14	28.1	0.71	8.1	0.174
	ROI-2	0.18	0.20	28.1	0.71	13.8	0.742
	ROI-3	0.27	0.36	28.4	0.70	20.2	0.880
	ROI-4	0.50	0.61	28.3	0.70	39.2	0.965
	ROI-5	0.69	0.91	28.4	0.70	45.8	0.984

points are the smoothed experimental waveforms, for various damping levels. The continuous curve is

$$\phi_1(x, t) = 1 + Hcn^2[2K(k)ft; k], \quad (3)$$

which is Eq. (1) evaluated at a specific value of x . Using only one free parameter, k , we fit our experimental data to Eq. (3) by minimizing chi-squared.

The fitted curves match the experimental waveforms well. This agreement was found not only for Fig. 3, (for ROI-3 and five gas pressures), but also for all the data we tested. This agreement is seen for waves with small and large amplitudes alike. At large amplitude (i.e., at low pressure), the features of sharpened peaks and flattened bottoms are captured well by the cnoidal wave solution, Eq. (3). We should mention one small feature in the experimental waveform that is not captured by the cnoidal solution. There is a very small but detectable skewness in the wave trough in Fig. 3(a) and 3(b).

This agreement leads us to conclude that the cnoidal wave solution can accurately describe the waveform of nonlinear dust acoustic waves in experimental data. Having thus confirmed the usefulness of the cnoidal solution, we can now turn our attention to practical uses for it. In particular, we will evaluate the parameter k in the cnoidal formula, as a useful measure of wave's nonlinearity.

B. Measures of nonlinearity

Beyond previous experimental measures of a wave's nonlinearity, such as the percentage of density fluctuation or the total harmonic distortion THD, we find here that the elliptic parameter k is also useful for quantifying the wave's nonlinearity. This parameter is obtained experimentally as the free parameter in the fitting.

As expected, we find that k increases with increasing nonlinearity, as can be seen in Fig. 3. For the largest wave amplitudes, the nonlinear waveform has sharpened peaks and a flattened bottom, and in that case we find that k has a large value of 0.997, which is close to the theoretical maximum of unity. On the other hand, for small wave amplitudes in Fig. 3(e), the waveform is almost sinusoidal, and the parameter k has a smaller value 0.88. In Fig. 4(a) the parameter k is shown as a function of wave amplitude.

For comparison, we also calculate the total harmonic distortion (THD),

$$\text{THD} = \sqrt{\frac{A_2^2 + A_3^2}{A_1^2}}. \quad (4)$$

Here, A_1 , A_2 , and A_3 are the amplitudes of the fundamental, second, and third harmonics of the waves; they are obtained from a Fourier transformation of raw waveforms. The parameter THD was previously used to

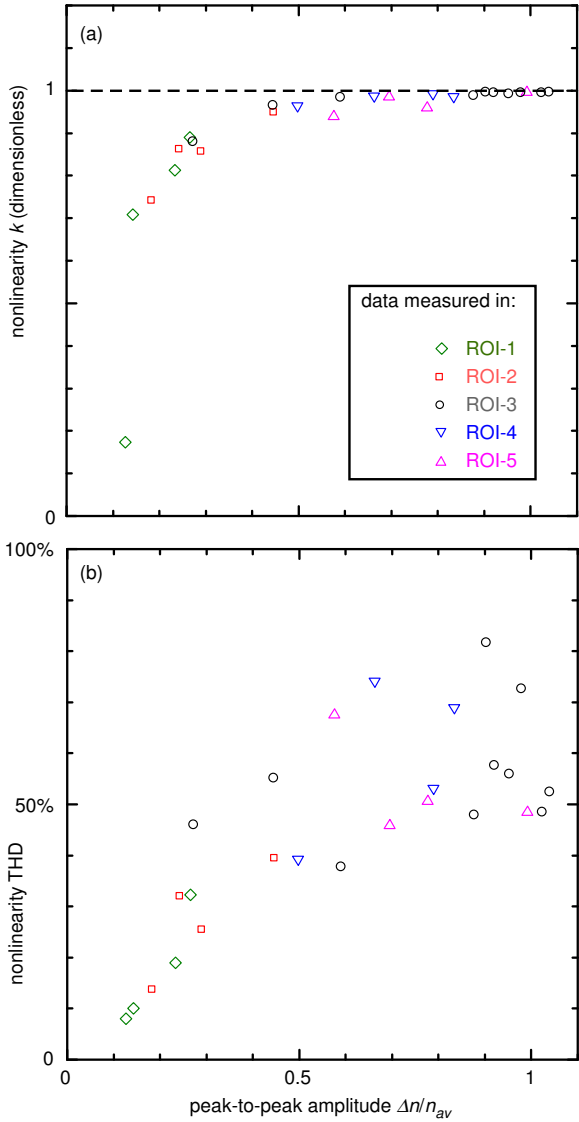


FIG. 4. Measures of the wave's nonlinearity. The nonlinearity is quantified by (a) the elliptic parameter k , and (b) the total harmonic distortion THD. The peak-to-peak amplitude Δn is normalized by a time-average density n_{av} , not by the undisturbed dust density n_0 . Data shown here are taken from Table I. Each data point corresponds to one pressure and one ROI. (For each symbol there is more than one data point because we used various values of the gas pressure.) Note that the parameter k in (a) reaches its theoretical maximum of unity and no longer varies as wave amplitude $\Delta n/n_{av} \gtrsim 0.4$, while THD in (b) exhibits a monotonic trend that persists even at a higher wave amplitude.

characterize the nonlinearity of DAWs by Flanagan and Goree [24]. We do the same here, except that our formula Eq. (4) is a ratio of amplitudes instead of powers. Our results for THD are presented in Table I and Fig. 4(b).

We find that, as measures of nonlinearity, both k and THD exhibit monotonic trends, varying upward with wave amplitude, as the wave amplitude is increased from a low level. However, the sensitivity of these param-

eters is not the same. The parameter k exhibits most of its variation for relatively low amplitudes $\Delta n/n_{av} < 0.4$, as defined in Table I. For larger amplitudes, k reaches its theoretical maximum of unity. On the other hand, THD exhibits a monotonic trend that does not rapidly saturate at high wave amplitude. This comparison suggests that, as a quantitative indicator of wave's nonlinearity, the cnoidal elliptic parameter k has great sensitivity to the nonlinearity at relatively small wave amplitudes, while THD is more sensitive at larger amplitudes. Another difference is that THD exhibits larger scatter than for the parameter k .

VI. THEORETICAL DISCUSSION

A. The role of ions in the cnoidal theory

Next we will present a theoretical derivation to demonstrate that the cnoidal solution for nonlinear dust acoustic waves is robust. Since the basic nonlinear model equation, the KdV equation, always has a cnoidal solution, our key point here is that the KdV equation itself can be obtained for various assumptions about the ions. In the previous derivation of [44, 45] for DAWs, Yadav *et al.* assumed a Boltzmann ion response. Here we assume cold ions responding ballistically to the wave electric potential. Despite this change in the assumption, we still obtain a KdV equation, which admits a cnoidal wave solution.

We next briefly outline a derivation of the model KdV equation including the cold-ion response. We use a simple description of the dusty plasma system as being composed of three fluid components representing the dust, the ions and the electrons [15]. The dust dynamics is then given by,

$$\frac{\partial n}{\partial t} + \frac{\partial(nu)}{\partial x} = 0, \quad (5)$$

$$\frac{\partial u}{\partial t} + u \frac{\partial u}{\partial x} - \frac{Z_d e}{M_d} \frac{\partial \phi}{\partial x} = 0, \quad (6)$$

$$\frac{\partial^2 \phi}{\partial x^2} = -4\pi e(n_i - n_e - Z_d n). \quad (7)$$

Here, Eq. (5) is the dust continuity equation with n and u denoting the dust density and velocity respectively. Equation (6) is the dust momentum equation with ϕ representing the electrostatic potential, and Z_d and M_d being the dust charge and mass respectively. Equation (7) is the Poisson equation, with n_i denoting the ion density and n_e the electron density. Dust pressure is neglected (cold dust fluid). Since the electron mass is negligible compared to that of the massive dust particles it is appropriate to assume the electrons to obey a Boltzmann distribution,

$$n_e = n_{e0} \exp\left(\frac{e\phi}{T_e}\right). \quad (8)$$

A similar assumption of a Boltzmann response for ions was of Yadav *et al.* [44], but this assumption will likely lead to an exaggerated variation in ion density. This is so in part because of the low ion temperature T_i in a gas discharge plasma. In general, T_i in such a plasma is smaller than 0.1 eV. There is evidence, from nonlinear DAW experiments similar to ours [51], that the wave's potential can vary with an amplitude of 0.1 V or more. Such a small ion temperature combined with a large excursion of wave potential would cause a large change in ion density. In fact, besides the ion thermal energy, there is also the energy associated with ion flow, and the latter is generally much greater in the sheath region of a gas discharge plasma. The ion flow velocity must be large, comparable to the ion acoustic speed, as described by the Bohm sheath criterion. The cooling effect of neutral gas acting on the ions, however, can cause a temperature ratio $T_i/T_e \ll 1$, so that the ion thermal velocity is low. For these gas discharge conditions, a more reasonable approximation for modeling the change in ion density due to a variation in electric potential can be made by a ballistic approximation.

A different approximation for the ions, which results in a much smaller variation in the ion density, is the cold-ion 'ballistic response model.' This description neglects ion kinetic effects, and describes the ions with just two hydrodynamic parameters that can vary in response to the wave: a local ion density n_i and a local ion fluid velocity v_i . The fluid equations for ions are

$$n_i v_i = n_{i0} v_{i0} \quad (9)$$

$$\frac{m_i v_i^2}{2} + e\phi = \frac{m_i v_{i0}^2}{2} \quad (10)$$

where m_i is the ion mass, and v_{i0} is the equilibrium ion streaming velocity.

Quasi-neutrality at equilibrium gives,

$$n_{i0} = n_{e0} + Z_d n_0. \quad (11)$$

A linear dispersion relation can be obtained by a linear perturbation analysis of Eqs. (5) to (11), with perturbations $\exp[i(qx - \omega t)]$, yielding

$$\begin{aligned} \omega^2 &= \beta^2 C_s^2 q^2 \left[1 + \frac{q^2 \lambda_D^2}{1 - \eta \delta} \right]^{-1} \\ &\approx \beta^2 C_s^2 q^2 \quad (\text{for } q^2 \lambda_D^2 \ll 1), \end{aligned} \quad (12)$$

where $\beta^2 = Z_d(\delta - 1)/(1 - \eta\delta)$, $C_s = (T_e/M_d)^{1/2}$, $\delta = n_{i0}/n_{e0}$, $\eta = T_e/(m_i v_{i0}^2)$ and $\lambda_D = (T_e/4\pi n_0 e^2)^{1/2}$.

The KdV equation can be obtained by employing the stretched variables,

$$\xi = \epsilon(x - u_{ph}t) ; \quad \tau = \epsilon^3 t.$$

[If this were done at the lowest order of the perturbation, the analysis would yield the linear dispersion relation of Eq. (12).] To include nonlinear terms, one retains terms of the next significant order, giving the following nonlinear evolution equation for the perturbed potential (or density or velocity),

$$\frac{1}{u_{ph}} \frac{\partial \phi_1}{\partial \tau} + \frac{1}{2} \left[\frac{\delta \eta^2 - 1}{1 - \eta \delta} - 3 \frac{Z_d}{\beta^2} \right] \phi_1 \frac{\partial \phi_1}{\partial \xi} + \frac{\lambda_D^2}{2Z_d} \frac{\delta - 1}{1 - \eta \delta} \frac{\partial^3 \phi_1}{\partial \xi^3} = 0, \quad (13)$$

where $u_{ph} = \beta C_s$ is the linear phase velocity. Equation (13) has the form of the KdV equation, a fully integrable nonlinear PDE, which has many exact analytic solutions including the well known soliton solutions. There is a difference, in comparing Eq. (13) to Eq. (12) of Yadav *et al.* [44], in the details of the coefficients. An exact periodic solution of the KdV equation, Eq. (13), is a chain of solitons, of the form given by Eq. (1).

B. Wave amplitude

Two chief approximations are made in the derivation of the KdV equation Eq. (13): weak dispersion and weak nonlinearity. The weak dispersion approximation is justified for dust acoustic waves since they have long wavelengths ($q\lambda_D \ll 1$). The weak nonlinearity condition, which needs a more detailed examination, requires the normalized perturbed quantities to be small, because

the derivation of KdV equation involves an expansion of quantities such as wave potential and dust density in terms of an expansion parameter ϵ . In contrast to the linear dispersion relation, which retains only terms of order ϵ , the derivation of the KdV equation retains higher order terms. For example, terms of order $\epsilon = 3/2, 5/2$, and 2 are retained in the dust continuity equation, dust momentum equation, and Poisson's equation, respectively.

For the normalized wave potential, $e\phi/T_e$, the weak nonlinearity condition is probably well satisfied. We estimate that $e\phi/T_e$ is of order 0.1 for this experiment. This estimate is based on experimental determination of values, in a separate but similar experiment [51], of ϕ in the range 0.12 to 0.26 V, and an electron temperature measured as [51] $T_e = 3$ eV or even higher values [24].

For dust density, perturbations can be larger than for other physical parameters. The highly charged dust has a strong response to an electric field, even if singly charged electrons and ions do not. For this reason, the weak non-

linearity condition is not always satisfied for the dust, in our experiments. In particular, during portions of the waveforms in the runs at low gas pressure, the dust density fluctuation briefly attains fairly high levels, as indicated in Table I.

Our experimental result in Fig. 3, that there is good agreement with the cnoidal waveform, is particularly interesting. The cnoidal waveform is found to be reasonably accurate even beyond its intended application, under weak nonlinearity condition assumed by the KdV equation.

A further theoretical step can improve upon the KdV model by including higher orders in the perturbation expansion. The result of this generalization is an extended KdV equation [52, 53]; although this equation is not fully integrable, it still has an exact cnoidal wave solution [53] of the form Eq. (3) used in our present analysis. This point suggests the cnoidal waveform is accurate beyond the applicability of the KdV equation and may help explain the excellent theoretical fit to the experimental data, even at high amplitude.

VII. CONCLUSION

We find that the cnoidal wave solution of Eq. (1) accurately describes the waveform of nonlinear dust acoustic waves in a ground-based experiment. This finding is based on our analysis of experimental waveforms of

dust particle's number density, which are found to be fitted well by the cnoidal solution over a wide range of amplitudes. This agreement is found even at fairly large amplitudes for the dust density perturbations, suggesting that the cnoidal solution is reasonably accurate even beyond the weak-nonlinearity conditions that are assumed by the KdV equation.

The fit yields a useful measure for the wave's nonlinearity, the so-called elliptic parameter k . We find that the parameter k is useful for waves at smaller amplitude. For larger amplitude, the total harmonic distortion THD is found to be a more useful indicator.

We believe it will be interesting to further test the cnoidal wave solution, using the data in other dusty plasma experiments, including PK-4 instrument on the International Space Station [54]. Such experiments, under microgravity conditions, do not require a large vertical electric field, thus have a lesser ion flow.

VIII. ACKNOWLEDGMENTS

Work at Iowa was supported by NASA-JPL subcontracts 1579454 and 1573629, DOE and NSF. Work at NRL supported by NASA-JPL subcontract 1573108. A.S. thanks the Indian National Science Academy (INSA) for their support under the INSA Senior Scientist Fellowship scheme.

-
- [1] H. Thomas, G. E. Morfill, V. Demmel, J. Goree, B. Feuerbacher, and D. Mohlmann, *Phys. Rev. Lett.* **73**, 652 (1994).
 - [2] J. H. Chu and L. I, *Phys. Rev. Lett.* **72**, 4009 (1994).
 - [3] A. Melzer, A. Homann, and A. Piel, *Phys. Rev. E* **53**, 2757 (1996).
 - [4] W. T. Juan and Lin I, *Phys. Rev. Lett.* **80**, 3073 (1998).
 - [5] P. K. Shukla and A. A. Mamun, *Introduction to Dusty Plasma Physics* (Institute of Physics, Bristol, 2002).
 - [6] B. Liu, J. Goree, V. Nosenko, and L. Boufendi, *Phys. Plasmas* **10**, 9 (2003).
 - [7] Y. Feng, J. Goree, and B. Liu, *Rev. Sci. Instrum.* **78**, 053704 (2007).
 - [8] O. Ishihara, *J. Phys. D: Appl. Phys.* **40**, R121 (2007).
 - [9] A. Melzer and J. Goree, in *Low Temperature Plasmas: Fundamentals, Technologies and Techniques*, 2nd ed., edited by R. Hippler, H. Kersten, M. Schmidt, and K. H. Schoenbach (Wiley-VCH, Weinheim, 2008), p. 129.
 - [10] G. E. Morfill and A. V. Ivlev, *Rev. Mod. Phys.* **81**, 1353 (2009).
 - [11] V. E. Fortov and G. E. Morfill, *Complex and Dusty plasma: From Laboratory to Space in Series in Plasma Physics* (CRC Press, New York, 2009).
 - [12] T. M. Flanagan and J. Goree, *Phys. Rev. E* **80**, 046402 (2009).
 - [13] A. Piel, *Plasma Physics* (Springer, Heidelberg, 2010).
 - [14] M. Bonitz, C. Henning, and D. Block, *Rep. Prog. Phys.* **73**, 066501 (2010).
 - [15] N. N. Rao, P. K. Shukla, and M. N. Yu, *Planet. Space Sci.* **38**, 543 (1990).
 - [16] A. Barkan, R. L. Merlino, and N. D'Angelo, *Phys. Plasmas* **2**, 3563 (1995).
 - [17] R. L. Merlino, A. Barkan, C. Thompson, and N. D'Angelo, *Plasma Phys. Control. Fusion* **39**, A421 (1997).
 - [18] C. Thompson, A. Barkan, N. D'Angelo, and R. L. Merlino, *Phys. Plasmas* **4**, 2331 (1997).
 - [19] V. I. Molotkov, A. P. Nefedov, V. M. Torchinskii, V. E. Fortov, and A. G. Khrapak, *JETP* **89**, 477 (1999).
 - [20] R. L. Merlino, A. Barkan, C. Thompson, and N. D'Angelo, *Phys. Plasmas* **5**, 1607 (1998).
 - [21] J. Pramanik, B. M. Veerasha, G. Prasad, A. Sen, and P. K. Kaw, *Phys. Letts. A* **312**, 84 (2003).
 - [22] P. Bandyopadhyay, G. Prasad, A. Sen, and P. K. Kaw, *Phys. Letts. A* **368**, 491 (2007).
 - [23] A. Piel, O. Arp, M. Klindworth, and A. Melzer, *Phys. Rev. E* **77**, 026407 (2008).
 - [24] T. M. Flanagan and J. Goree, *Phys. Plasmas* **17**, 123702 (2010).
 - [25] T. M. Flanagan and J. Goree, *Phys. Plasmas* **18**, 013705 (2011).
 - [26] R. L. Merlino, *Phys. Plasmas* **16**, 124501 (2009).
 - [27] R. L. Merlino, J. R. Heinrich, S. H. Kim, and J. K. Meyer, *Plasma Phys. Control. Fusion* **54**, 124014 (2012).
 - [28] W. D. Suranga Ruhunusiri and J. Goree, *Phys. Rev. E* **85**, 046401 (2012).

- [29] J. D. Williams, IEEE Trans. Plasmas **41**, 788 (2013).
- [30] W. D. Suranga Ruhunusiria and J. Goree, Phys. Plasmas **21**, 053702 (2014).
- [31] R. L. Merlino, J. Plasma Phys. **80**, 773 (2014).
- [32] M. Rosenberg, G. J. Kalman, S. Kyrkos, and Z. Donko, J. Phys. A: Math. Gen. **39**, 4613 (2006).
- [33] J. H. Chu, J.-B. Du, and L. I, J. Phys. D: Appl. Phys. **27**, 296 (1994).
- [34] G. E. Morfill, H. M. Thomas, U. Konopka, H. Rothermel, M. Zuzic, A. Ivlev, and J. Goree, Phys. Rev. Lett. **83**, 1598 (1999).
- [35] K. O. Menzel, O. Arp, D. Caliebe, and A. Piel, IEEE Trans. Plasma Sci. **38**, 838 (2010).
- [36] K. O. Menzel, O. Arp, and A. Piel, Phys. Rev. Lett. **104**, 235002 (2010).
- [37] K. O. Menzel, O. Arp, and A. Piel, Phys. Rev. E **83**, 016402 (2011).
- [38] B. L. Méhauté, D. Divoky, and A. Lin, *Proceedings of the 11th International Conference on Coastal Engineering* (American Society of Civil Engineers, New York, 1969), Chap. 7, pp. 86-107.
- [39] W. J. Pierson, Jr., M. A. Donelan, and W. H. Hui, J. Geophys. Res. **97**, 5607 (1992).
- [40] U. Kauschke and H. Schlüter, Plasma Phys. Control. Fusion **33**, 1309 (1991).
- [41] H. Schamel, Plasma Phys. **14**, 905 (1972).
- [42] N. Korneev, A. A. Iribeb, V. A. Vysloukhm, and M. A. Basurto Pensado, Opt. Commun. **197**, 209 (2001).
- [43] T. Soomere, R. Pöder, K. Rannat, and A. Kask, Proc. Estonian Acad. Sci. Eng. **11**, 245 (2005).
- [44] L. L. Yadav and R. Bharuthram, AIP Conf. Proc. **649**, 483 (2002).
- [45] L. L. Yadav, S. V. Singh, and R. Bharuthram, J. Plasma Phys. **75**, 697 (2009).
- [46] T. K. Baluku, M. A. Hellberg, I. Kourakis, and N. S. Saini, Phys. Plasmas **17**, 053702 (2010).
- [47] S. L. Jain, R. S. Tiwari, and M. K. Mishra, Phys. Plasmas **19**, 103702 (2012).
- [48] M. Ishak-Boushaki, D. Djellout, and R. Annou, Phys. Plasmas **19**, 073707 (2012).
- [49] N. S. Saini and P. Sethi, Phys. Plasmas **23**, 103702 (2016).
- [50] R. E. Tolba, W. M. Moslem, A. A. Elsadany, N. A. El-Bedwehy, and S. K. El-Labany, IEEE Trans. Plasma Sci. **45**, 2552 (2017).
- [51] W. D. Suranga Ruhunusiri, Ph.D. thesis, the University of Iowa, 2014.
- [52] A. H. Khater, M. M. Hassan, and R. S. Temshah, Mathematics and Computers in Simulation **70**, 221 (2005).
- [53] E. Infeld, A. Karczewska, G. Rowlands, and P. Rojmej, Acta Physica Polonica A **133**, 1191 (2018).
- [54] M. Y. Pustynnik, M. A. Fink, V. Nosenko, T. Antonova, T. Hagl, H. M. Thomas, A. V. Zobnin, A. M. Lipaev, A. D. Usachev, V. I. Molotkov, O. F. Petrov, V. E. Fortov, C. Rau, C. Deysenroth, S. Albrecht, M. Kretschmer, M. H. Thoma, G. E. Morfill, R. Seurig, A. Stettner, V. A. Alyamovskaya, A. Orr, E. Kufner, E. G. Lavrenko, G. I. Padalka, E. O. Serova, A. M. Samokutyayev, and S. Christoforetti, Rev. Sci. Instrum. **87**, 093505 (2016).